Journal of Alloys and Compounds 495 (2010) 254–259

Contents lists available at ScienceDirect

Journal of Alloys and Compounds

journal homepage: www.elsevier.com/locate/jallcom

# Preparation and microwave absorption properties of basalt fiber/nickel core–shell heterostructures

Yu-Qing Kang[a], Mao-Sheng Cao[a,*], Jie Yuan[b], Lu Zhang[a], Bo Wen[a], Xiao-Yong Fang[c]

[a] School of Materials Science and Engineering, Beijing Institute of Technology, Zhongguancun 5, Haidian District, Beijing 100081, PR China
[b] School of Information Engineering, Centre University for Nationality, Beijing 100081, PR China
[c] School of Science, Yanshan University, Qinhuangdao 066004, PR China

ARTICLE INFO

*Article history:*
Received 3 November 2009
Received in revised form 25 January 2010
Accepted 28 January 2010
Available online 6 February 2010

*Keywords:*
Composite materials
Electromagnetic properties
Microwave absorption properties

ABSTRACT

Basalt fiber/nickel core–shell heterostructures with different thicknesses of nickel shells are fabricated successfully. The electromagnetic parameters of basalt fiber/nickel-paraffin composites ranging from 8.2 to 12.4 GHz (X band) are measured for investigating the microwave absorption properties. The electromagnetic parameters of basalt fiber/nickel are several times higher than those of naked basalt fibers due to the formation of the core–shell interface. The measured results indicate that effective electromagnetic match is realized in the whole X band. The values of complex permittivity and permeability of basalt fiber/nickel increase monotonically with the increasing thicknesses of the nickel shells. It is interesting that the reflection loss of basalt fiber/nickel do not show the monotonic character with the increasing thicknesses of the nickel shells. The basalt fiber/nickel with the nickel shell thickness about 300 nm shows the strongest reflection loss. The value of reflection loss is more than 15 dB in the whole X band and reaches 40 dB at 8.9 GHz, while the naked basalt fibers hardly exhibit any microwave absorption. The excellent microwave absorption properties of the basalt fiber/nickel core–shell heterostructures are attributed to the good electromagnetic match between the dielectric loss and magnetic loss.



## 1. Introduction

With the development of radar and microwave communication technology, the study of microwave absorbing materials has attracted worldwide attention due to their applications in high-energy storage systems, electromagnetic interference shielding and radar systems [1–8]. In recent years, nanoscale structures, particularly one-dimensional (1D) nanostructures, provide a kind of interesting candidates for microwave absorbers [9–17]. Microwave absorption properties of materials are determined by the complex permittivity ($\varepsilon' - j\varepsilon''$), complex permeability ($\mu' - j\mu''$), electromagnetic impedance match, and their microstructures. Many research works have shown that these nanostructures represent high complex permittivity, particularly in low-frequency regions. A common point of view is that the space-charge polarization and interface polarization give rise to the high permittivity of nanostructures, due to large interface and high density of defects of the nanostructures [18–22]. Nevertheless, the imbalance of the electromagnetic parameter match is still an important problem to be solved. Generally, the excellent microwave absorption is believed to result from the efficient complementarities between the relative permittivity and permeability. Either only the dielectric loss or only the magnetic loss may induce weak microwave absorption due to the imbalance of the electromagnetic match [23]. For better electromagnetic match, ferromagnetic core–shell structures, such as CNTs/Fe [24,25], CNTs/$CoFe_2O_4$ [26], $Fe_3O_4/SnO_2$ [27], and ZnO-coated iron nanocapsules [28], have been fabricated by various methods [29–32]. The core–shell structures show the microwave absorption better than the pure core or shell materials [31,32]. However, the complicated fabrication process of these core–shell structures has been challenging for putting such core–shell structures into commercial applications. Therefore, it is significant to search other approaches to fabricate core–shell structures with excellent microwave absorption. In previous works, we have fabricated basalt fiber/nickel core–shell heterostructures and investigated the effect of the orientation of the heterostructures on the electromagnetic properties [33,34]. Based on these results, we fabricate basalt fiber/nickel core–shell heterostructures with different thicknesses of nickel shells and investigate their microwave absorption properties. Moreover, the corresponding mechanism is discussed.

## 2. Experimental

The basalt fibers with an average diameter of 9 μm and length of 1 cm were used in the experiment. According to previous works [33,35], the basalt fiber/nickel

* Corresponding author. Tel.: +86 10 68914062; fax: +86 10 68914062.
*E-mail addresses:* caomaosheng@bit.edu.cn (M.-S. Cao), yuanjie4000@sina.com (J. Yuan).

0925-8388/$ – see front matter © 2010 Elsevier B.V. All rights reserved.
doi:10.1016/j.jallcom.2010.01.143

core–shell heterostructures were fabricated via the following process: (1) Basalt fibers were pretreated prior to the deposition of nickel. In brief, 0.5 g basalt fibers were introduced into 200 mL HF/HCl solution, 200 mL $SnCl_2$ solution, and 200 mL $PdCl_2$ solution in sequence for 5 min for the deposition of Pd–Sn catalytic nuclei on the surface of basalt fibers. (2) The as-treated basalt fibers were dispersed in 200 mL reactive solution, which was composed of 0.25 M $NiCl_2{\cdot}6H_2O$, 0.09 M $NiSO_4{\cdot}6H_2O$, 0.084 M $NaH_2PO_2{\cdot}2H_2O$, 1.84 M $NH_4Cl$, and 0.09 M $Na_2C_6H_5O_7{\cdot}2H_2O$. The solution was adjusted to a pH value of ~9.0 by adding $NH_3{\cdot}H_2O$. And then the mixture was kept at 50 °C for the reaction process. The obtained fibers were washed several times with distilled water and dried at room temperature. The as-prepared samples were denoted by samples A, B and C for the reaction times 10, 20 and 30 min, respectively.

The structures of the naked basalt fibers and the basalt fiber/nickel were investigated by X-ray diffractometer (XRD, Rigaku, D/max-RB, Cu-Kα). The morphologies and components of the naked basalt fibers and the basalt fiber/nickel were characterized by a scanning electron microscope (SEM, HITACHI S-3500N), an energy dispersive spectrometer (EDS, OXFORD INCA) and an X-ray photoelectron spectroscope (XPS, PHI 5300, Mg-Kα). The electromagnetic parameters (complex permeability and complex permittivity) of the samples were measured in the X band (from 8.2 to 12.4 GHz) by an ANRITSU 37269D vector network analyzer. The samples used for the electromagnetic measurement were prepared by dispersing the naked basalt fibers and the basalt fiber/nickel (samples A–C), cut into about 3 mm into melting paraffin with a weight fractions of 10%, respectively. Then these mixtures were molded into a hollow pipe of a rectangular waveguide cavity with dimensions $22.9 \times 11.0 \times 2.7\ mm^3$ for the complex permittivity and complex permeability measurements. The distribution of the basalt fibers and the basalt fiber/nickel in the samples is random. The paraffin, with its dielectric constant of approximately 2.2 and dielectric loss tangent of about $1 \times 10^{-3}$, is an ideal candidate for an electromagnetic window material.

## 3. Results and discussion

### 3.1. Microstructure analysis

Fig. 1 shows the XRD patterns of the naked basalt fibers and the basalt fibers/nickel core–shell heterostructures. It is obvious that the diffraction peaks of nickel can be observed in the XRD pattern of the basalt fibers/nickel heterostructures. Fig. 2(a) shows the SEM image of the naked basalt fibers with smooth surfaces and Fig. 2(b) shows the morphologies of the basalt fiber/nickel core–shell heterostructures (sample B). It can be seen that the surfaces of the basalt fibers have been coated by uniform and continuous nickel shells. The section image of the basalt fiber/nickel core–shell heterostructures is shown in Fig. 2(c), which also indicates that the basalt fibers are coated by continuous nickel shells in thicknesses of about 100 nm. Fig. 2(d)–(f) shows the element maps of Ni, Si and O in the selected area in Fig. 2(c), respectively. The O-map is just the same as the Si-map and shows a circular feature, which clearly indicates that the oxygen originates from the basalt fibers. However, the Ni-map shows an annular feature, revealing that the nickel originates from the shells. The results demonstrate that the surfaces of the basalt fibers have been well coated by continuous and uniform nickel shells which are composed of pure nickel rather than its oxide. Fig. 3(a) shows the XPS of basalt fiber/nickel and the inset is a high-magnification SEM image of the nickel shells. The oxygen peaks and carbon peaks in the XPS in Fig. 3(a) come from the contamination of the XPS equipment. It is obvious that nickel peaks present in the XPS of basalt fiber/nickel core–shell heterostructures, but not in the XPS of naked basalt fibers, as shown in Fig. 3(b). The high-magnification SEM image indicates that the nickel shells are composed of nickel nanoparticles with diameters of about 15–65 nm.

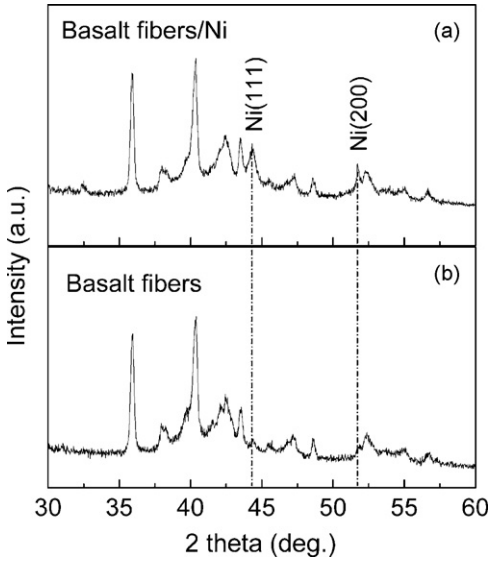


**Fig. 1.** XRD patterns of (a) basalt fiber/nickel core–shell heterostructures and (b) naked basalt fibers.

Fig. 4(a) shows the schematic illustration of the fabrication of basalt fiber/nickel core–shell heterostructures. Firstly, Pd–Sn catalytic nuclei are formed on the surfaces of the naked basalt fibers, which act as seeds for the deposition of Ni. Secondly, the basalt fibers with Pd–Sn catalytic nuclei are introduced into the chemical reaction solution, the redox reaction occurs on the Pd–Sn catalytic nuclei, and $Ni^{2+}$ is reduced to the metal nickel. Thirdly, the reduced nickel promotes the proceeding of the redox reaction as nickel is an autocatalytic metal, and the reduced nickel particles are adsorbed on the surfaces of the basalt fibers. Thus the basalt fiber/nickel core–shell heterostructures are formed. By adjusting the reaction time, the basalt fiber/nickel core–shell heterostructures with the nickel shells of different thicknesses can be successfully obtained. Fig. 4(b)–(d) shows the SEM images of samples A, B and C, respectively. The insets are the high-magnification SEM images. The average thicknesses of the nickel shells for samples A, B and C are approximately 70, 300 and 700 nm, respectively. The nickel shells are uniform and continuous. Even with only single 70-nm nickel shells coated on the surfaces of the basalt fibers (Fig. 4(b)), no obvious crack can be seen on the surfaces of nickel shells.

### 3.2. Electromagnetic properties of basalt fiber/nickel

The electromagnetic parameters of basalt fiber/nickel core–shell heterostructures as well as naked basalt fibers and paraffin composites are investigated in the X band. Fig. 5(a) shows the SEM image of basalt fiber/nickel-paraffin composites and Fig. 5(b) shows the fracture surface of the composites. It can be seen that the basalt fiber/nickel heterostructures disperse in the paraffin matrix randomly. The holes observed in Fig. 5(b) present as a result of the evulsions of basalt fiber/nickel during the preparing process. The electromagnetic parameters of naked basalt fibers and basalt fiber/nickel core–shell heterostructures are shown in Fig. 6. It is found that the electromagnetic parameters of basalt fiber/nickel are much higher than those of naked basalt fibers and are sensitive to the thicknesses of the nickel shells. The values of the complex permittivity ($\varepsilon'$ and $\varepsilon''$) increase explicitly with the increasing thicknesses of the nickel shells, as shown in Fig. 6(a) and (b). The $\varepsilon'$ value of naked basalt fibers has a constant of 2.35, slightly larger than that of the paraffin. The $\varepsilon'$ values of samples A and B decrease slightly with the increasing frequency, with average values of about 5 and 8, respectively. The $\varepsilon'$ value of sample C decreases from an initial high value of 25.6 to 12.2 as the frequency increases. The $\varepsilon''$ values of samples A–C are higher than 1 and the highest value of sample C reaches 19.47. The $\varepsilon''$ value of sample C exhibits a fluctuant feature with a reverse trend to $\varepsilon'$, i.e., $\varepsilon''$ gradually increases with $\varepsilon'$ decreasing when the frequency changes from 8.2 to 12.4 GHz. Even with only 70-nm nickel shells coated on the basalt fibers (sample A), $\varepsilon''$ is almost two order of magnitudes higher than that of naked basalt fibers (from ~0.05 to ~1). Fig. 6(c) and (d) shows the

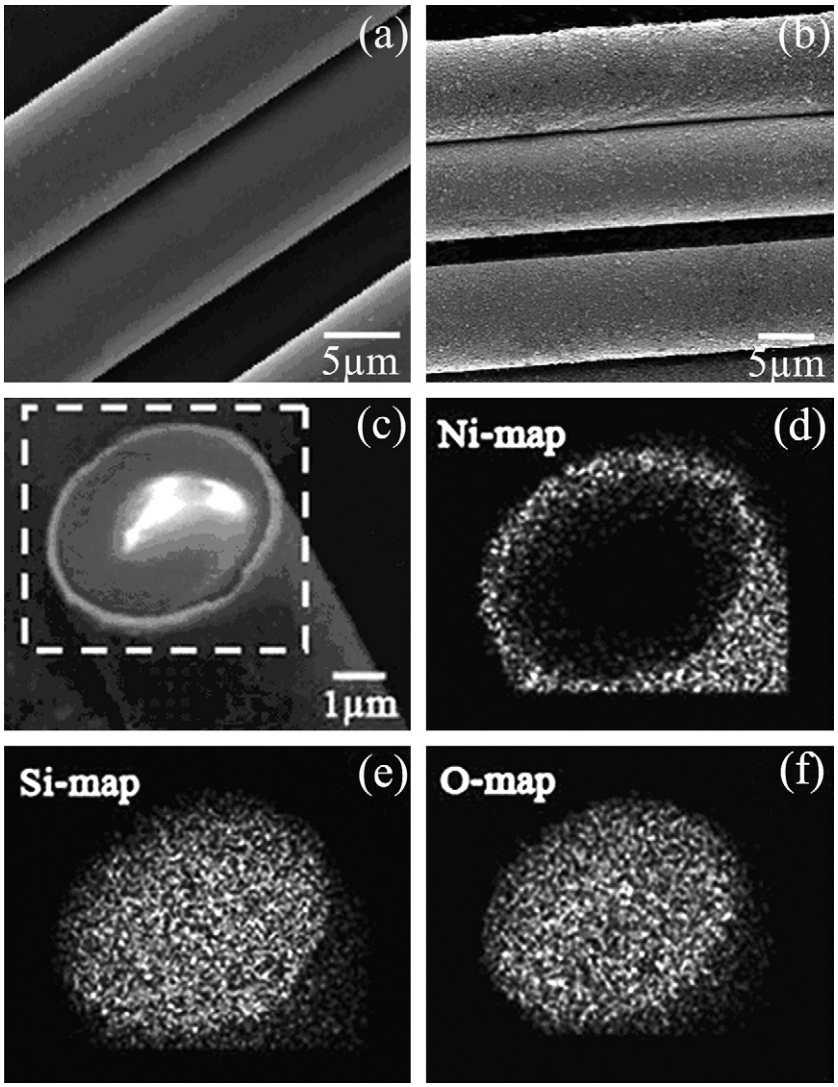


**Fig. 2.** SEM images of (a) naked basalt fibers and (b) basalt fiber/nickel core–shell heterostructures (sample B). (c) Cross-sectional image of the basalt fiber/nickel core–shell heterostructures. (d)–(f) Maps of nickel, silicon and oxygen of the selected area in (c).

complex permeability of naked basalt fibers and basalt fiber/nickel heterostructures. It can be seen that the real permeability $\mu'$ of the naked basalt fibers is approximately 1.0 and the imaginary permeability $\mu''$ is about 0.01, which indicates that the naked basalt fibers are nearly nonmagnetic. For samples A–C, $\mu'$ and $\mu''$ increase with the increasing thicknesses of the nickel shells, showing a similar trend with the permittivity. Based on the data in Fig. 6, we calculate the dielectric loss tangent $\tan\delta_e$ ($\varepsilon''/\varepsilon'$) and the magnetic loss tangent $\tan\delta_m$ ($\mu''/\mu'$), as shown in Fig. 7. Both $\tan\delta_e$ and $\tan\delta_m$ of basalt fiber/nickel heterostructures have been strongly enhanced as compared with that of the naked basalt fibers. Moreover, $\tan\delta_e$ and $\tan\delta_m$ of basalt fiber/nickel increase monotonically with the increasing thicknesses of the nickel shells. The values of $\tan\delta_e$ of basalt fiber/nickel are in the range of 0.15–1.57, depending on the frequency and thicknesses of nickel shells, whereas those of $\tan\delta_m$ are in the range of 0.04–0.19. This reveals that the basalt fiber/nickel heterostructures are high-loss materials and effective complementarities between the dielectric loss and the magnetic loss are realized.

In general, two mechanisms are considered to be responsible for the nature of frequency-dependent permittivity of the "core–shell"-type nanocomposites: space-charge polarization and dipole polarization [36,37]. Space-charge polarization is caused by charge accumulation at the heterogeneous interface and is more prominent at lower frequencies. In the basalt fiber/nickel heterostructures, dipole polarization is the major mechanism for permittivity enhancing. Dipole polarization is lossy and leads to the increase of complex permittivity of the basalt fiber/nickel heterostructures. Moreover, according to the dielectric theory, crystal lattice defects will lead to electron relaxation polarization in the external electric field by forming weak bound electrons. For nickel particles with particle sizes of about 15–65 nm, there are lots of defects on the surfaces of nanoparticles such as dislocations, vacancies and dangling bonds. These defects may lead to electron relaxation polarization, which will attenuate electromagnetic wave. As a consequence, the values of complex permittivity of basalt fiber/nickel heterostructures are much higher than that of the naked basalt fibers. It is clear that the complex permeability of the basalt fiber/nickel heterostructures originate from the nickel shells rather than the basalt fibers. As we know, nickel is a ferromagnetic metal and magnetization occurs in the nickel particles in the external electromagnetic field. The easy magnetization direction of the nickel particles is along the depositional direction of the nickel shells. During the magnetization process, magnetic domain form an

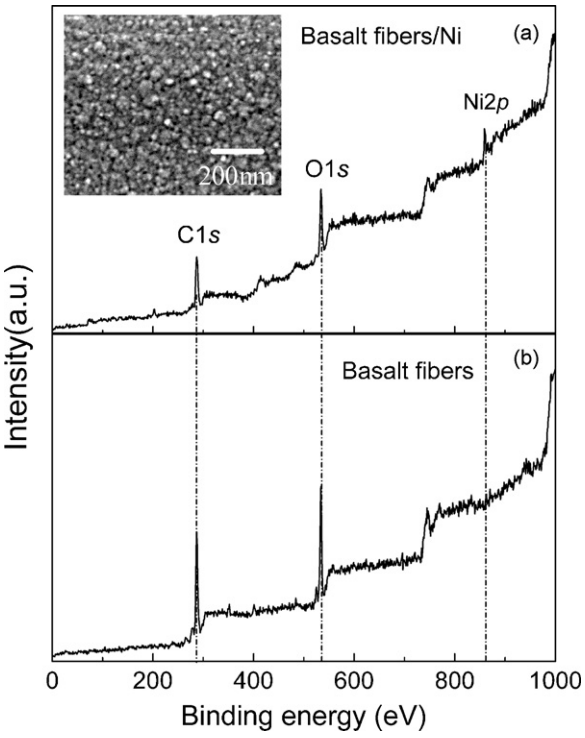


**Fig. 3.** XPS of (a) basalt fiber/nickel core–shell heterostructures and (b) naked basalt fibers. Inset in (a) is the high-magnification SEM image of the nickel shell.

array along the depositional direction of the nickel shells. However, small thicknesses of the nickel shells may resist the magnetization process, which may lead to the increase of the magnetic loss. Thus, the basalt fiber/nickel heterostructures show a good electromagnetic match, which is favorable for the microwave absorption properties.

### 3.3. Microwave absorption properties of basalt fiber/nickel

The reflection losses $R_L$ of the naked basalt fibers and samples A–C is calculated by the following equations based on the transmit-line theory [38]:

$$z_{in} = \sqrt{\frac{\mu_r}{\varepsilon_r}} \tanh\left[j\left(\frac{2\pi}{c}\right)\sqrt{\frac{\mu_r}{\varepsilon_r}} fd\right], \quad (1)$$

$$R_L(\text{dB}) = 20\log\left|\frac{z_{in}-1}{z_{in}+1}\right|, \quad (2)$$

where $Z_{in}$ is the normalized input impedance, $c$ is the velocity of electromagnetic waves in free space, $f$ is the frequency of microwaves, and $d$ is the thickness of the absorber (in our case, $d$ = 3 mm). The calculated results of $R_L$ are shown in Fig. 8. It is clear that the naked basalt fibers hardly exhibit any microwave absorption. However, $R_L$ increases obviously when the basalt fibers are coated by the nickel shells with thicknesses of about 70 nm (sample A), 300 nm (sample B) and 700 nm (sample C). For sample A, $R_L$ is more than 10 dB in the range of 9.2–12.4 GHz and increases up to nearly 20 dB. $R_L$ of sample C is in the range of 5.3–7.9 dB in the whole frequency investigated. However, $R_L$ of sample B is more than 15 dB in the whole X band and reaches 40 dB at 8.9 GHz, which is better than or comparable to those of CNT/Fe nanocomposites [24,25], $Fe_3O_4/SnO_2$ core/shell nanorods [27], hollow glass spheres/nickel core/shell composite [39] and Ni/C nanocapsules [40]. The excellent

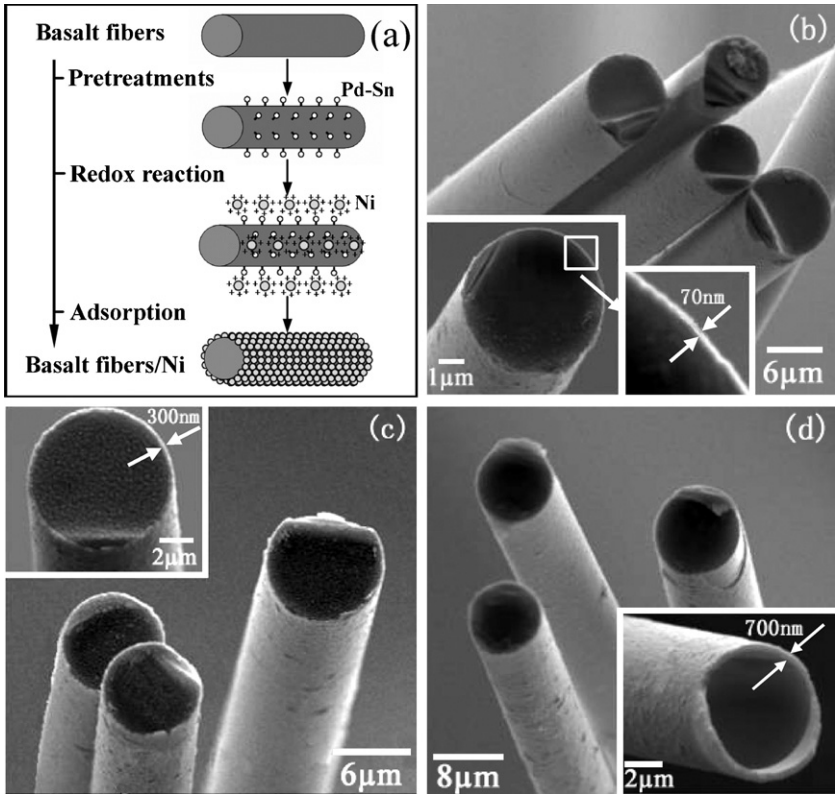


**Fig. 4.** (a) Schematic illustration of fabrication for basalt fiber/nickel core–shell heterostructures. (b)–(d) SEM images of samples A–C.

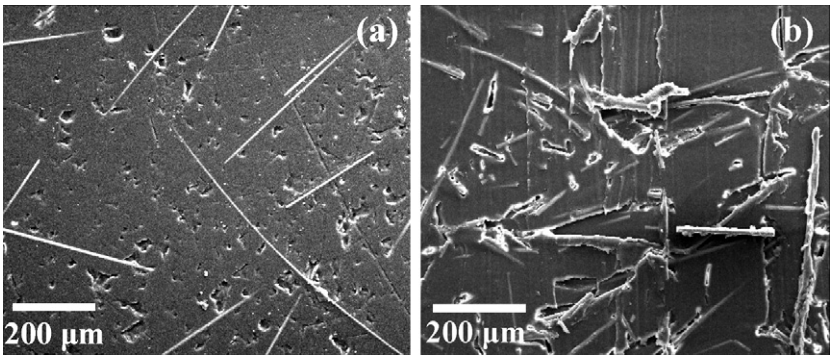


**Fig. 5.** SEM images of (a) basalt fiber/nickel-paraffin composites and (b) fracture surface of the composites.

microwave absorption properties of basalt fiber/nickel core–shell heterostructures are attributed to the effective complementarities between the dielectric loss and the magnetic loss as described above. It is interesting that $R_L$ of basalt fiber/nickel does not increase monotonically with the increasing thicknesses of the nickel shells. According to the impedance match condition, the electromagnetic parameters corresponding to A (dB) attenuation are as follows [41]:

$$\varepsilon' = \frac{\pi c}{2d\omega} c \tanh\left(\frac{\pi}{2}\tan\delta_e\right)\frac{1-10^{-A/20}}{1+10^{-A/20}}, \quad (3)$$

$$\varepsilon'' = \varepsilon' \times \tan\delta_e = \frac{\pi c \tan\delta_e}{2d\omega} c \tanh\left(\frac{\pi}{2}\tan\delta_e\right)\frac{1-10^{-A/20}}{1+10^{-A/20}}, \quad (4)$$

$$\mu' = \frac{\pi c}{2d\omega}\tanh\left(\frac{\pi}{2}\tan\delta_m\right)\frac{1+10^{-A/20}}{1-10^{-A/20}}, \quad (5)$$

$$\mu'' = \mu' \times \tan\delta_m = \frac{\pi c \tan\delta_m}{2d\omega}\tanh\left(\frac{\pi}{2}\tan\delta_m\right)\frac{1+10^{-A/20}}{1-10^{-A/20}}, \quad (6)$$

where $\omega = 2\pi f$ is the angular frequency and $f$ is the measurement frequency. From Eqs. (3)–(6), it is clear that $A$ (dB) is the coupling results of thickness, frequency and electromagnetic parameters. In this case, complex interaction occurs between the basalt fiber/nickel heterostructures and high-frequency electromagnetic wave. Therefore, different thicknesses of nickel shells cause different electromagnetic parameters for samples A–C, as shown in Fig. 6. The change of the frequency-dependent electromagnetic parameters may lead to the deviation of the impedance matching condition. Thus, $R_L$ of basalt fiber/nickel heterostructures do not show any monotonic character with the increasing thicknesses of the nickel shells. The results demonstrate that the basalt fiber/nickel core–shell heterostructures will be good candidates for applications in microwave absorption devices.

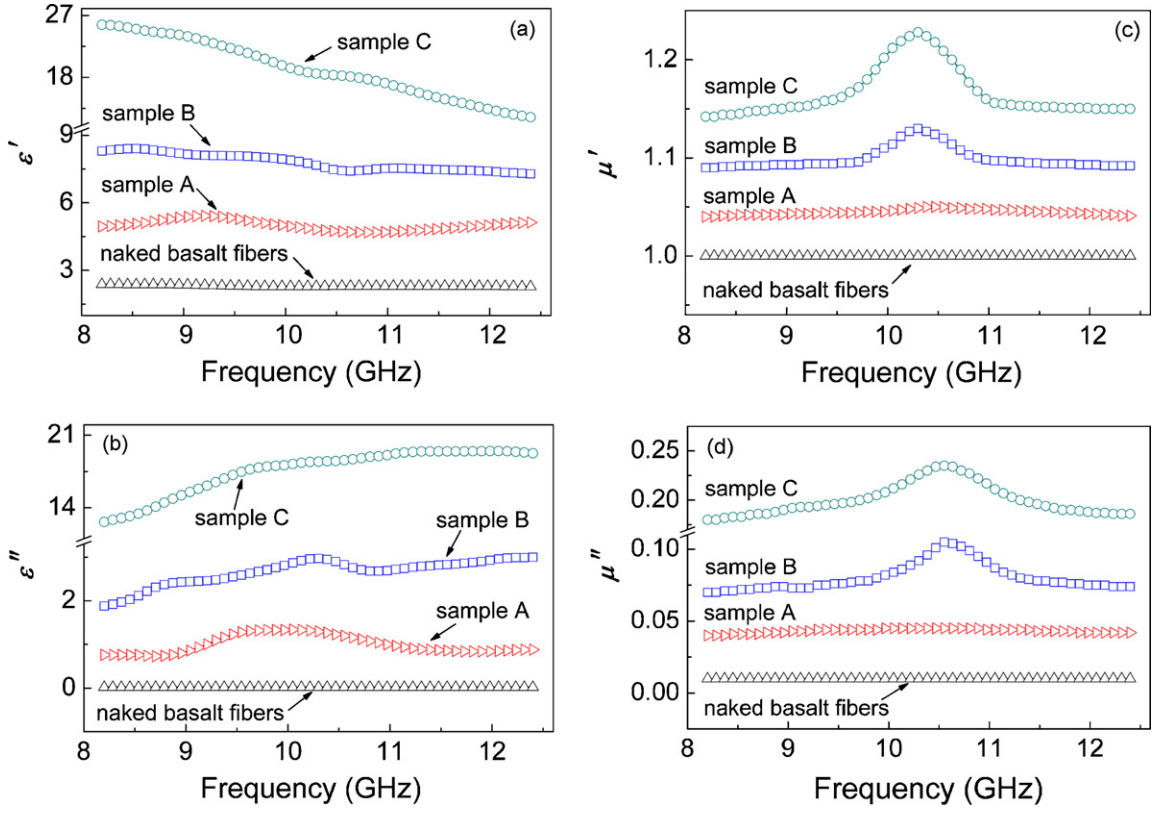


**Fig. 6.** Electromagnetic parameter of naked basalt fibers (up-triangles), samples A (right-triangles), B (squares), and C (circles) in X band: (a) real and (b) imaginary part of permittivity, (c) real and (d) imaginary part of permeability.

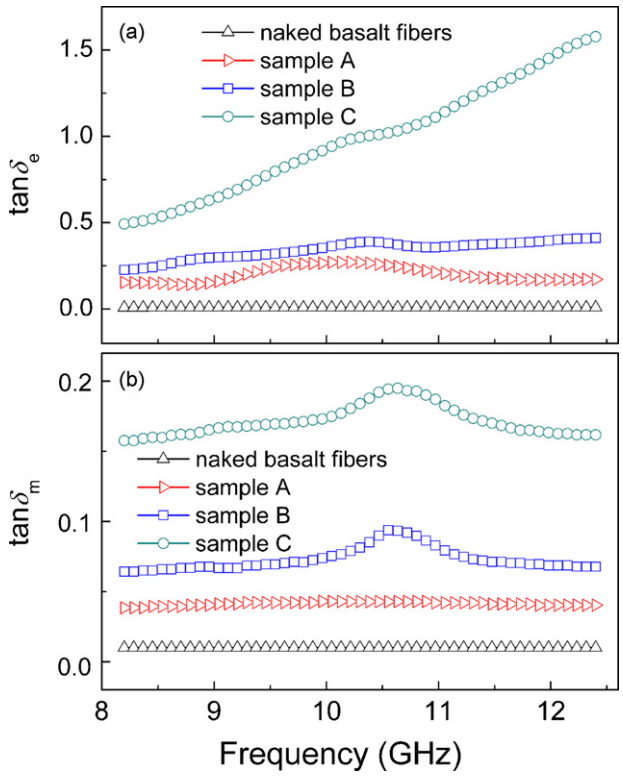


**Fig. 7.** (a) Dielectric loss tangent tan $\delta_e$ and (b) magnetic loss tangent tan $\delta_m$ of naked basalt fibers (up-triangles), samples A (right-triangles), B (squares), and C (circles) in X band.

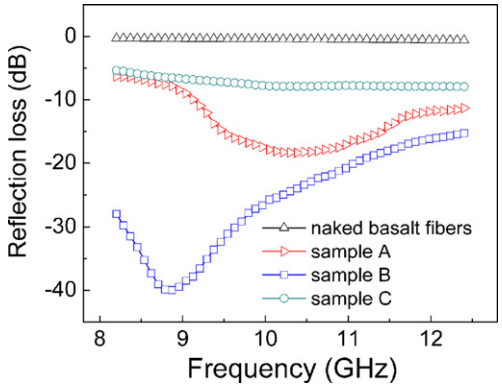


**Fig. 8.** Reflection loss of naked basalt fibers (up-triangles), samples A (right-triangles), B (squares), and C (circles) in X band. The thickness of absorber is 3 mm.

## 4. Conclusions

In summary, we have fabricated basalt fiber/nickel core–shell heterostructures with different thicknesses of the nickel shells and investigated the microwave absorption properties of basalt fiber/nickel heterostructures. The electromagnetic parameters of basalt fiber/nickel have been greatly enhanced as compared with that of the naked basalt fibers. The basalt fiber/nickel core–shell heterostructures present high reflection loss, while the naked basalt fibers hardly exhibit any microwave absorption. It is interesting that the reflection loss of basalt fiber/nickel does not show monotonic character with the increasing thicknesses of nickel shells, whereas electromagnetic match plays an important role in microwave absorption of basalt fiber/nickel core–shell heterostructures. The basalt fiber/nickel core–shell heterostructures with dielectric cores and ferromagnetic shells may become attractive for applications of microwave absorptive materials.

## Acknowledgements

This work was financially supported by the National Natural Science Foundation of China under Grant Nos. 50972014 and 50872159, and the National Defense Research Projects of China under Grant No. A2220061080. The authors also thank the English Editor J.-L. Wu for the revision.

## References

[1] R.F. Zhuo, L. Qiao, H.T. Feng, J.T. Chen, D. Yan, Z.G. Wu, P.X. Yan, J. Appl. Phys. 104 (2008) 094101.
[2] Y.K. Liu, Y.J. Feng, X.W. Wu, X.G. Han, J. Alloys Compd. 472 (2009) 441–445.
[3] S.B. Ni, X.H. Wang, G. Zhou, F. Yang, J.M. Wang, D.Y. He, J. Alloys Compd. 489 (2010) 252–256.
[4] M.S. Cao, X.L. Shi, X.Y. Fang, Z.L. Hou, H.B. Jin, Y.J. Chen, Appl. Phys. Lett. 91 (2007) 203110.
[5] S. Sugimoto, T. Maeda, D. Book, T. Kagotani, K. Inomata, M. Homma, H. Ota, Y. Houjou, R. Sato, J. Alloys Compd. 330–332 (2002) 301–306.
[6] Y.Q. Kang, M.S. Cao, J. Yuan, X.L. Shi, Mater. Lett. 63 (2009) 1344–1346.
[7] J. Zeng, J.C. Xu, P. Tao, W. Hua, J. Alloys Compd. 487 (2009) 304–308.
[8] M.S. Cao, W.L. Song, Z.L. Hou, B. Wen, J. Yuan, Carbon 48 (2010) 788–796.
[9] F. Tabatabaie, M.H. Fathi, A. Saatchi, A. Ghasemi, J. Alloys Compd. 474 (2009) 206–209.
[10] F. Tabatabaie, M.H. Fathi, A. Saatchi, A. Ghasemi, J. Alloys Compd. 470 (2009) 332–335.
[11] R.F. Zhuo, H.T. Feng, L. Qiao, J.Z. Liu, J.T. Chen, D. Yan, J.J. Feng, H.J. Li, S. Cheng, B.S. Geng, X.Y. Xu, J. Wang, Z.G. Wu, P.X. Yan, G.H. Yue, J. Phys. D: Appl. Phys. 41 (2008) 185405.
[12] R.F. Zhuo, H.T. Feng, J.T. Chen, D. Yan, J.J. Feng, H.J. Li, B.S. Geng, S. Cheng, X.Y. Xu, P.X. Yan, J. Phys. Chem. C 112 (2008) 11767–11775.
[13] X.L. Shi, M.S. Cao, X.Y. Fang, J. Yuan, Y.Q. Kang, W.L. Song, Appl. Phys. Lett. 93 (2008) 223112.
[14] D. Yan, S. Cheng, R.F. Zhuo, J.T. Chen, J.J. Feng, H.T. Feng, H.J. Li, Z.G. Wu, J. Wang, P.X. Yan, Nanotechnology 20 (2009) 105706.
[15] G.Z. Zou, M.S. Cao, H.B. Lin, H.B. Jin, Y.Q. Kang, Y.J. Chen, Powder Technol. 168 (2006) 84–88.
[16] G.Z. Zou, M.S. Cao, L. Zhang, H. Xu, Z.P. Wang, J. Inorg. Mater. 21 (2006) 781–797.
[17] D.L. Zhao, Q. Lv, Z.M. Shen, J. Alloys Compd. 480 (2009) 4634–4638.
[18] X.L. Su, W.C. Zhou, Z.M. Li, F. Luo, H.L. Du, D.M. Zhu, Mater. Res. Bull. 44 (2009) 880–883.
[19] X.L. Su, W.C. Zhou, F. Luo, Z.M. Li, D.M. Zhu, J. Alloys Compd. 476 (2009) 644–647.
[20] X.S. Fang, C.H. Ye, T. Xie, Z.Y. Wang, J.W. Zhao, L.D. Zhang, Appl. Phys. Lett. 88 (2006) 013101.
[21] W.L. Song, M.S. Cao, Z.L. Hou, X.Y. Fang, X.L. Shi, J. Yuan, Appl. Phys. Lett. 94 (2009) 233110.
[22] W.L. Song, M.S. Cao, Z.L. Hou, J. Yuan, X.Y. Fang, Scr. Mater. 61 (2009) 201–204.
[23] A. Wadhawan, D. Garrett, J.M. Perez, Appl. Phys. Lett. 83 (2003) 2683–2685.
[24] R.C. Che, L.M. Peng, X.F. Duan, Q. Chen, X.L. Liang, Adv. Mater. 16 (2004) 401–405.
[25] D.L. Zhao, X. Li, Z.M. Shen, J. Alloys Compd. 471 (2009) 457–460.
[26] R.C. Che, C.Y. Zhi, C.Y. Liang, X.G. Zhou, Appl. Phys. Lett. 88 (2006) 033105.
[27] Y.J. Chen, P. Gao, R.X. Wang, C.L. Zhu, L.J. Wang, M.S. Cao, H.B. Jin, J. Phys. Chem. C 113 (2009) 10061–10064.
[28] X.G. Liu, Y.D. Geng, H. Meng, P.J. Shang, Z.D. Zhang, Appl. Phys. Lett. 92 (2008) 173117.
[29] Y.J. Chen, P. Gao, C.L. Zhu, R.X. Wang, L.J. Wang, M.S. Cao, X.Y. Fang, J. Appl. Phys. 106 (2009) 054303.
[30] X.L. Shi, M.S. Cao, J. Yuan, Q.L. Zhao, Y.Q. Kang, X.Y. Fang, Y.J. Chen, Appl. Phys. Lett. 93 (2008) 183118.
[31] X.A. Li, X.J. Han, Y.J. Tan, P. Xu, J. Alloys Compd. 464 (2008) 352–356.
[32] R. Sharma, R.C. Agarwala, V. Agarwala, J. Alloys Compd. 467 (2009) 357–365.
[33] Y.Q. Kang, M.S. Cao, X.L. Shi, Z.L. Hou, Surf. Coat. Technol. 201 (2007) 7201–7206.
[34] Y.Q. Kang, M.S. Cao, J. Yuan, X.Y. Fang, Chin. Phys. B 19 (2010) 017701.
[35] G.Z. Zou, M.S. Cao, L. Zhang, J.G. Li, H. Xu, Y.J. Chen, Surf. Coat. Technol. 201 (2006) 108–112.
[36] Z. Han, D. Li, X.G. Liu, Y.D. Geng, J. Li, Z.D. Zhang, J. Phys. D: Appl. Phys. 42 (2009) 055008.
[37] R. Ravindran, K. Gangopadhyay, S. Gangopadhyay, N. Mehta, N. Biswas, Appl. Phys. Lett. 89 (2006) 263511.
[38] E. Michielssen, J. Sajer, S. Ranjithan, R. Mittra, IEEE Trans. MicrowaVe Theory Technol. 41 (1993) 1024–1031.
[39] Z.G. An, S.L. Pan, J.J. Zhang, J. Phys. Chem. C 113 (2009) 2715–2721.
[40] X.F. Zhang, X.L. Dong, H. Huang, Y.Y. Liu, W.N. Wang, X.G. Zhu, B. Lv, J.P. Lei, C.G. Lee, Appl. Phys. Lett. 89 (2006) 053115.
[41] M.S. Cao, R.R. Qin, C.J. Qiu, J. Zhu, Mater. Design 24 (2003) 391–396.